J. Non-Crystalline Solids, 357:2046–2053, 2011.

Aggregation model for the gelation of a *sol* starting from the processing conditions

F. A. Campo, J. S. Rivas Murillo, E. J. Barbero[1]
Mechanical and Aerospace Engineering, West Virginia University,
Morgantown, WV 26506-6106, USA

Abstract

A stochastic computational model for the gelation of a *sol* is explained and tested for the case of neutral silica aerogels. The computational model produces the final structure of the *sol* after gelation, using two of the several physical phenomena occurring during gelation of *sols*. Diffusion, represented by Brownian motion, is modeled by a random walk, and chemical reactions are incorporated through a stochastic aggregation model using a probability function; the later determined in terms of the processing conditions based on the knowledge of the cluster formation energies. The two phenomena are coupled by a Monte Carlo simulation. The analysis of the connected structure and its functionality is demonstrated for neutral silica aerogels. It is shown how the gelation process can be controlled to obtain different structures for different application requirements. The only parameters required by the model are the density and the processing conditions. The results of the model show that those parameters strongly affect the structure of the generated samples. Therefore, processing conditions could be selected to produce aerogels with structures tailored to specific applications, which would constitute a major achievement in aerogel fabrication.

Keywords

Gelation; Monte Carlo simulation; Aerogels; Fractal structures; Computational model.

1 Introduction

Sol-Gel technologies include a range of processes which start with a metal alkoxide solution, and lead to products such as dense films, aerogels, dense ceramics, uniform particles, and ceramic fibers**?**. Many of these products are made by producing first a *sol*, which is the metal alkoxide solution with activated reactions of hydrolysis and condensation. The *sol* gelates into a *wet gel*, which is composed of a nanoporous solid network immersed in a liquid phase (solvent). The solid network can be separated from the solvent by evaporation of the liquid which leads to xerogels, or by supercritical drying which leads to aerogels. Supercritical drying does not break the fine solid structure present in the wet gel, thus imparting aerogels with unique physical properties**??**. Because of their unique physical properties, aerogels have found applications in insulation, catalysts, sensors, fuel storage,

[1]Corresponding author. The final publication is available at http://dx.doi.org/10.1016/j.jnoncrysol.2011.02.025

Cherenkov detectors, lightweight optics, special effect optics, impedance matchers for transducers, energy absorbers, hypervelocity particle traps, ICs, and capacitors**??????????**.

The structural characteristics of aerogels, therefore their properties, are mostly defined during the gelation of the *sol*. Processing conditions as temperature, pressure, the nature of the catalyst, and the ratio of precursor:catalyst:solvent, have a mayor impact on how the structure is formed **??**. Although it is well known that the gelation process is a fundamental part of aerogel fabrication, it is not completely understood **???**. In this paper, the process of formation of aerogel structures is investigated. A general computational model for the gelation of a *sol* and the formation of the aerogel structure is proposed. The results of this gelation model are verified for the case of silica aerogels. The resulting model can be used to predict the processing-property relationships for a *sol gel* derived material.

Different models have been proposed to describe the structure of aerogels. Some are based on experimental evidence, mostly scattering experiments, which work under the assumption that the structure is fractal **?????**. However, the fractal model is not always applicable **??**. Other models, based on Percolation Theory (PT), allow to visualize the gelation when the network percolates **??**. Additional tests can be done to the structures generated with PT, however, the predictions do not correlate well with experimental data for aerogels **??**. Aggregation models, which are modified versions of PT models, can incorporate physical phenomena such as Brownian Motion (BM), reactions, or both combined **????????**. In limiting cases, aggregation models produce similar results to PT models **?**. Aggregation models generate structures that resemble aerogels **??**, however, the parameters of the models have not been directly related to the processing conditions. In this paper, the input parameters for the model are determined in terms of the processing conditions for aerogels, which allows us to use the computational model to predict the processing-property relatioships for aerogels.

Other techniques such as molecular dynamics (MD) and *ab-initio* simulations have been used to create clusters of silica and aerogels **???????** evaluating their response to different types of stimuli. However, these techniques do not allow the control of the features of the structure generated, and the formation process cannot be directly related to the processing conditions.

2 Aggregation model

The aggregation model proposed assumes that the gelation process consists of two physical phenomena: diffusion of particles in the *sol*, which can be described by a Brownian motion (BM) and condensation reactions that occur when the clusters collide. Hydrolysis is assumed to occur fast[2], which guarantees the presence of reactive particles from the beginning of the simulation. The algorithm allows to include the rate of hydrolysis incorporating a source of reactive particles, but that is not considered here since only the competition between the browinian motion and the condensation of particles in the aggregation process is investigated. Also sintering and aging could also be investigated but these additional processes are out of the scope of the aggregation process.

Through a Monte Carlo (MC) simulation **??**, the different phenomena are modeled and coupled together. For this, each phenomena is associated to a set of possible events. The set of events to model the BM are differentiated from the reactions by the existence or not of a collision. Only when a collision occurs, a reaction can occur, but no BM occurs. The algorithm starts by choosing a particle and a tentative direction of movement. Next, the algorithm evaluates if the cluster containing the particle collides or not with any other particle of the system. If no collision is detected, the cluster

[2]There is evidence, for acidic conditions that hydrolysis reactions occur at least one order of magnitude faster than condensation reactions**?**.

can move in the tentative direction reproducing BM. If a collision is detected, the cluster will stay at the same position, but it opens the possibility for a reaction to occur [3]. Next, the algorithm tests if a reaction occurs between the test particle and the target particle [4]. If there is no reaction, the cycle is repeated as described in the flow chart in figure 1.

The Metropolis algorithm **?** is used to choose random events from the set of events that characterize each phenomenon, satisfying the physical laws and statistical mechanics. This algorithm is congruent to the Boltzmann postulate **?** which states that events at the same energy level occur with the same probability. In this way, all the events of the BM are equally probable to occur because there is no net change of the total energy of the system. The problem of BM is discussed in detail in section 2.1.

The Metropolis algorithm sorts the events based on the difference in the total energy (from a reference) of the system ΔH as it happens for reactions. For the set of all possible reactions that can occur, the probability of the k-th reaction to occur is given by

$$P^k_{Metro} = \frac{1}{Z} e^{-\frac{\Delta H_k}{k_b T}} \tag{1}$$

where k_b is the Boltzmann constant, T is the temperature of the system, and Z is the partition function for the reactions defined as

$$Z = \sum_j e^{-\frac{\Delta H_j}{k_b T}} \tag{2}$$

In the section 2.2, reactions are discussed and related to the processing conditions through the energies of formations of the clusters, which can be directly related to the reaction energies ΔH_k.

2.1 Brownian Motion

The BM is modeled stochastically by a random walk on a simple cubic lattice. The simple cubic lattice, defined by a lattice parameter length, implies that a particle located at a site can have a maximum of six particles in its vicinity, therefore, a particle can have a maximum of six bonded particles to it. The random walk consists on randomly choosing a cluster to move to its vicinity. A particular cluster is chosen to move when a particle that makes part of the cluster is chosen using a probability function. The probability function for all the particles in the i-th cluster, P_{BMi}, is defined using the Einstein and Smoluchowski theory **??**. This theory measures the drag by the medium of the cluster using an effective radius a_i calculated in terms of its total surface area A_i from $A_i = 4\pi a_i^2$. A_i is calculated summing up, over all the particles of the cluster, all the sites in the vicinity of each particle without bonded particles to it, and multiplying by the primary particle size squared. Additionally, since the event of moving a whole cluster implies moving at once not only the particle that was chosen but all the particles associated to its cluster, the probability function is divided by the number of particles of the cluster, m_i. Finally, normalizing the probability function with a partition function Z_{BM} over all the possible particles that could be randomly chosen, P_{BMi} is written as

$$P_{BMi} = \frac{1}{Z_{BM}} \frac{1}{m_i a_i^{3/2}} \tag{3}$$

[3] The colliding particle in the moving cluster is called test particle. The particle that is hit by the test particle is the target particle.

[4] Multiple simultaneous colliding sites are possible. In this case, the reaction probability is divided by the number of simultaneous collisions to account the reduction in the intensity (pressure) of the collision.

where

$$Z_{BM} = \sum_k \frac{1}{m_k a_k^{3/2}} \tag{4}$$

Although (3) does not include the processing conditions of the *sol* explicitly, the probability function is the result of the diffusivity (or viscosity), which are temperature dependent. The explicit dependence on temperature is canceled in the normalization, unless the temperature is not constant through the system. The only parameters that explicitly appear in the normalized P_{BMi} in (3) are those that differentiate the clusters from each other, i.e., their sizes.

2.2 Reactions

The chemical reactions to aggregate particles are incorporated to the MC simulation when collisional events occur during the BM. If a collision occurs, a bond can form, which is equivalent to say that a reaction took place. The event of occurrence of a reaction is determined by the probability function P_{React}, that depends on the change of total energy of the system, ΔH, following the Metropolis algorithm in (1). ΔH can be measured at the states of the system after and before the reaction. In this way, calculating the total energy of the system for each state allows us to calculate ΔH_k between all the possible reactions, each one identified by the subscript k.

The total energy of formation for all the possible cluster formations can be found experimentally using calorimetry and spectroscopy such as Nuclear Magnetic Resonance **??**, or computationally using MD simulations and Quantum Mechanics calculations **?????**. The calculation of the energy of the system, requires the energy of formation of the clusters and the clusters present in the solution. The energy of formation of the clusters is highly dependent on the conditions of the solution, i.e., the processing parameters for the solution. These parameters are the temperature and the concentration ratio of the species involved in the process. For this study, to show how the model works, the formation energies of several clusters are taken from **?**. The data in **?** corresponds to a single processing condition, but the model can be applied to other conditions, simply by changing the energy of formation of the clusters.

The processing condition of **?** are summarized in Table 1. Since no catalyst was added, these conditions yield a neutral silica aerogel. The energy of formation E_c of the clusters shown in figure 2 are presented in the table 2. The nomenclature q_n^m, as it was introduced in **?**, means that the cluster has n silicon atoms which have m bonded silicons (by oxygen bridges). Based on these data, the change of the total energy, ΔH_k, of the clusters due to a reaction (labeled as k) can be calculated as follows.

First, note that in a single reaction, only two particles have a change in their energy. The other particles remain untouched, thus, note that the change of the total energy is solely due to the change of the energy of the colliding particles. This suggests to model the total energy of the clusters, E_c, as a summation of the energies of the individual particles, E_i that compose each cluster, and to consider the energy of each particle dependent only on its state, which is described by the *coordination number*, i.e. the number of bonds that the particle has.

Two models to describe the total energy of the clusters after a reaction are proposed here,

- *Model 1*: Each particle has an energy E_i which depends on its coordination number n_c. Therefore, the energy of a particle is one of the set $\{E_1, E_2, E_3, E_4\}$. Only four states are considered for the silica system since silicon can at most form four bonds. The energy required for five or six bonds is too high, therefore improbable.

- *Model 2*: E_i linearly increases with n_c as

$$E_{n_c} = a_1 + n_c a_2$$

where the value of a_1 is the energy associated with the existence of a particle, and it can be related to the chemical potential of the system at the processing conditions. The value of a_2 is the energy associated with the reduction of surface area due to the bonding between particles, related to the surface tension in the liquid-solid system (see sect. 2.2.1 for a refined model). Note how Model 2 is a simplified version of Model 1.

Knowing the formation energies of several clusters allows us to calculate the best fitting values of $\{E_1, E_2, E_3, E_4\}$, and a_1 and a_2. The parameters are found by the minimizing the error of a model

$$[M]\,\vec{p} = \vec{E_c} \tag{5}$$

where $[M]$ is the matrix of the coefficients of the equations in table 2 (based on Models 1 and 2), $\vec{p}$ is the vector with the parameters of the model, and $\vec{E_c}$ is the vector containing the formation energies given in column 2 of table 2 . The results of the fitting are presented in figure 3. The errors between the formation energy of the clusters predicted from reaction models 1 and 2, and the values calculated in **?** are shown in figure 4. The error decreases quickly as the size of the cluster (number of silicon atoms) increases. As a result, for the processing condition described in table 1, model 1 shows an increase in the energy associated to particles as its coordination number increases, which is in good agreement with the linear model 2. From now on, only model 2 is considered because it correctly captures the description of the energies of formation of the cluster under the mentioned processing conditions, and it is simpler than Model 1.

Two colliding particles forming a bond increase their coordination number n_c by one. Therefore, the change of total energy of the system (for each new bond), ΔH_{AB}, due to the reaction for the two colliding clusters, tagged as A and B, is

$$\begin{aligned} \Delta H_{AB} &= \Delta H_A + \Delta H_B \\ &= (E_{Af} - E_{Ao}) + (E_{Bf} - E_{Bo}) \end{aligned} \tag{6}$$

Using the Metropolis algorithm (1)

$$P_{React} = \frac{1}{Z} e^{-\frac{\Delta H_A}{k_b T}} e^{-\frac{\Delta H_B}{k_b T}} \tag{7}$$

According to model 2, ΔH_{AB}, due to the reaction for the two colliding clusters is,

$$\Delta H_{AB} = 2a_2 \tag{8}$$

which allows us to conclude that P_{React} is a constant since a_2 is a constant.

2.2.1 Refined Model

As observed above, P_{React} is constant under the processing conditions presented in table 1 (from **?**), but that may not be always the case**?**. What would happen if the processing conditions are modified? It becomes a daunting task to get all the possible reaction energies, ΔH_{AB}, for all the possible processing conditions, and to analyze the different types of structures that could appear.

Instead, a model for ΔH_{AB} is proposed here in order to study the structures parametrically. For a material system where every additional bond on a particle i requires more energy than the previous one (having a coordination number n_{ciA}), the change in total energy of each cluster A due to the reaction can be calculated as

$$\Delta H_A = a_2 + \widehat{w} n_{ciA} \tag{9}$$

where $\widehat{w}$ represents the extra energy needed (or the unused energy) to bond two particles compared to the linear model. The effective surface energy, $\widehat{a_2} = a_2 + \widehat{w} n_{ci}$, is no longer a constant. As a result, if (9) is put into the probability of the Metropolis algorithm in (7), P_{React} becomes,

$$\begin{aligned} P_{React} &= \frac{1}{Z} e^{-\frac{a_2+\widehat{w}n_{cA}}{k_b T}} e^{-\frac{a_2+\widehat{w}n_{cB}}{k_b T}} \\ &= \frac{1}{Z} e^{-\frac{2a_2}{k_b T}} e^{-\frac{\widehat{w}n_{cA}}{k_b T}} e^{-\frac{\widehat{w}n_{cB}}{k_b T}} \\ &= \frac{1}{\widehat{Z}} w^{n_{cA}} w^{n_{cB}} \end{aligned} \tag{10}$$

Since $\widehat{Z} = Z e^{\frac{2a_2}{K_B T}}$ is constant, and defining the reactivity as $w = e^{-\frac{\widehat{w}}{K_B T}}$, the probability of reaction can be written as a function of the reactivity. Note that for particular case of $\widehat{w} = 0$, $w = 1$, and P_{React} is a constant, matching the processing condition and the cluster formation energies calculated in **?** and given in table 1.

The final expression in (10) is similar to the one used by **?** with the difference that *functionality* was used in **?** instead of the coordination number to calculate P_{React}. The coordination number counts the formation of bonds for a particle. Therefore, this parameter accounts the energy state of the particle. On the other hand, the functionality, defined as the number of particles that are in the vicinity, bonded or not, is not directly related to the energy state. As it is shown (section 3), the functionality and coordination number distributions are different for the same structure. Furthermore, the response of the structure correlates with either functionality or coordination number distribution, as it is the case of density and elastic response, respectively. This becomes crucial for tailoring a material for a particular application, when it is desired to optimize one property or another.

3 Generated Sol Structures

Two structures with 251 and 1326 particles with simulation box length 10 and 20, respectively, were simulated to achieve densities[5] of $2200\left[kg/m^3\right] \cdot (251)/10^3 = 552.2\left[kg/m^3\right]$ and $2200\left[kg/m^3\right] \cdot (1326)/20^3 = 364.65\left[kg/m^3\right]$. These two samples where chosen to satisfy the relationship given by a fractal dimension, $D = 2.4$, as found experimentally for neutral aerogles **?**. Since only one particle fits in a simulation box size of the lattice parameter, $(N(1) = 1)$, the number of particles satisfy (11) from where the number of particles were calculated for reasonable computer simulation time.

$$N(L) = L^D \tag{11}$$

The simulation box length, which is dimensionless, can be converted to real length units by multiplying the lattice parameter length of $0.4\,nm$ **?** estimated by scattering experiments. Periodic

[5]The density of amorphous silica is $2200\left[kg/m^3\right]$.

boundary conditions are used for the algorithm, and the reported error is the standard deviation calculated from 24 samples.

The structure percolates when the correlation length is chosen equal to or greater than the size of the simulation box as evidenced in the slice presented in figure 5, for the reactivity chosen to reproduce neutral silica aerogels with the processing conditions of table 1. Percolating means that the formed structure spans the entire system**?**. The simulation box length is also the correlation length which measures the size of the clusters **?** for networks that percolate **?**.

The number of coordination distribution and the functionality distribution are presented in figures 6 and 7. All particles aggregated into a single cluster congruent with a 0% of isolated particles. If there were isolated particles, the percentage of 0-coordination number, and 0-functionality number would be different from 0.

The coordination (n_c) and functionality (f) distributions measure different aspects of the structure evidenced by the different results obtained in figures 6 and 7. The n_c distribution shows how the structure is connected. 35% of the structure consists of dead ends, i.e. particles with a single bond. Another 35%, with $n_c = 2$, are particles that act as elbows and linear bridges. Higher coordination numbers associated to branches are less likely to be seen, explaining an average coordination number of 2.0. The f distribution shows something different but not contradictory. Mostly all particles are surrounded by 2, 3, or 4 particles making it a compact structure explaining an average functionality of 2.8.

Next, when the correlation length is chosen much smaller than the size of the simulation box, the simulation yields aggregates that not percolate. The initial density is chosen to be lower than the one predicted for a correlation length corresponding to the size of the simulation box. When the system aggregates, locally the density increases creating isolated clusters that not percolate. Due to the nature of the simulated aggregation process when the aggregates do not percolate, it is thus possible to study the structure without adverse influence of the boundary conditions.

The influence of the size of the simulation box on the aggregation process is considered simulating systems with 20, 30, 40, 100 and 400 particles while keeping the same density. There is no significant difference between the n_c distributions when varying the number of particles while maintaining the initial density[6] for a single reactivity as presented in figure 8. The coordination number distribution behaves similarly to that of a denser sample as compared to figure 6.

The f distribution changes with the number of particles maintaining the initial density constant as presented in the figure 9. The percentage of 1 and 2 functionality numbers decrease with the increase of the number of particles, while for 4, 5, and 6 functionalities, the percentage increases. This translates into a more compact structure with the increase of the number of particles.

Furthermore, the effect of the density[7] is explored by modeling systems with dimensionless density of $40/10^3$, $100/10^3$, $200/10^3$, $400/10^3$, $706/10^3$ for a constant size of the simulation box. Changing the density of the samples does not cause a significant difference in the n_c distribution as it is showed in figure 10. Again, the n_c distribution resembles the one in figure 6. However, the f distribution is affected by the initial density as shown in figure 11. The functionality distribution is shifted towards higher functionality as the density is increased creating more compact structures. The same effect occurs in figure 7.

Additionally, the algorithm is used to investigate the different structures achieved by varying the reactivity. The n_c and f distributions are investigated for reactivities of 0.05, 0.2, 0.4, 0.6, 0.8, 1.0, 1.2, 1.4, 1.6 for a constant dimensionless density of $40/40^3$.

[6]The initial density used here is defined as the ratio of the number of particles and the volume of the simulation box because as the simulation evolves, the density is no longer uniform in space.

[7]The real density is equal to the dimensional density times the mass of amorphous silica that occupies the volume of the primary particle.

The coordination number and functionality distributions are presented in figures 12 and 13, respectively. There is a significant difference in coordination number distributions for different reactivities. The same happens for the functionality distributions, however, the amount of triple-coordinated particles increases reaching a maximum at $w = 0.8$, and then decreases. For tetra-, penta-, and hexa-coordinated particles the tendency is not completely clear, but they seem to follow the same trend as triple-coordinated particles for higher reactivities. The f distribution behaves with a similar trend as the n_c distribution, but the values in the coordination number distributions seem to be higher compared to the functionality distribution for lower numbers (almost doubled for $n_c = 1$ compared to $f = 1$), while they seem to be lower for higher numbers.

4 Discussion

Coordination number and functionality distributions shown in figures 6 and 7, respectively, measure different information about the structure of the neutral silica aerogel. The different responses of the structure, such as the mechanical response and the scattering of a coherent beam, depend on the connected structure or the mass distribution, respectively. However, the invariance in the results for different simulation box lengths scaling the number of particles with (11) are evidence of the fractal structure as result of the aggregation process.

The samples in figures 6, 7, 8, 9, 10, and 11 were chosen to observe the structure of neutral silica. The functionality tends to be higher than the coordination number in average. For very large samples, with low density and large correlation lengths, it is expected that the functionality distribution converges to the coordination number distribution. However, the functionality tends to be higher, meaning that not all of the particles in the vicinity of a particle are bonded to it. This also means that for the critical density when the system still percolates, the structure can arrange into a configuration conserving the correlation number distribution that minimizes energy with the minimum density given by the functionality distribution.

Achieving a lower density than the critical in a percolating structure would mean the development of a different coordination number distribution during the aggregation process which no longer minimizes the energy. So, in this case of lower densities, scattered clusters appear without percolating. Each cluster will have a correlation number distribution which minimizes the energy. On the contrary, a higher density implies the allocation of the excess of particles into the remaining spaces, intertwining the forming clusters, affecting the functionality distribution, shifting the average towards higher numbers. Nevertheless, the minimization of the energy is satisfied by the invariance of the correlation number distribution.

Invariance of the coordination number and functionality distributions for the neutral silica samples is presented in the figure 6 and 7. For the bigger sample, whose simulation box is twice as large, each part of the structure is connected and positioned in a similar way as its parts. In other words, if a part of the structure is taken, it will resemble the structure generated with less particles, i.e. a subpart with box length 10 of the sample with box length 20, resembles the simulation with box length 10. This is evidence of the fractal (self-affine) structure of neutral silica aerogles which is replicated with the aggregation model proposed here. The invariance of the coordination number distribution remains as long as the reactivity is fixed (as observed in figures 6, 8, and 10), which is valid too for samples whose correlation length is smaller than the size of the simulation box.

In contrast, the f distribution changes as presented in figures 9, and 11. In figure 9, the density is constant by increasing the number of particles and the size of the box. As the clusters are aggregating, bigger clusters react with bigger clusters leaving bigger spaces. To reach the same density at a large scale, the clusters must be denser (or more compact) compared to the case with

less particles. In other words, since the scale jump in a larger system is greater than in a smaller system (L is larger), the vacancies that appear by the aggregation of the clusters are compensated by more compact structures as the result of the apparent reduced volume available perceived by the particles when a cluster with empty spaces is formed. This explains how larger functionality numbers appear for larger number of particles for the same initial density. In figure 11 a similar effect is seen, but directly related to the addition of more particles that must be fitted in the spaces as the density is incremented for the same simulation box.

Combined, figure 9 and 11 explain figure 7. Since **?** found a decreasing relationship of the density with the correlation length ($\rho \propto L^{-1/1.67}$), the system creates empty spaces to cope with the decreasing density. In contrast to the previous cases, the reduction of the density is stronger than the reduction of the density explained by the spaces created by the aggregation of big clusters, so the structure needs to create less compact configurations as the correlation length, L, is increased.

Additional processes can be used to make the coordination number distribution converge to the functionality distribution for higher densities, creating the missing bonds. Aging and sintering applied to the structure as gelled, allow to create missing bonds between the particles and its neighbors. The f distribution is fixed during these processes since the functionality does not depend on bonding. In fact, the f distribution becomes the limit of the n_c distribution as the number of bonds is increased. So, aged and sintered structures will have the same f and n_c distributions, and only one distribution is enough to characterize them.

Changing the reactivity of the process to generate samples with constant density produced interesting results (figures 12 and 13). The reactivity determines which types of reactions are more prone to occur, favoring more linear structures for lower reactivities as presented in figure 12. In this way, for low reactivities, about 80% of the particles are elbows or linear structures. A more branched structure is formed as the reactivity is increased, first, raising the percentage of 3-coordinated particles, and then, for higher reactivities, higher order coordination numbers become more important. Note that for reactivities higher than 1, meaning $\widehat{w} < 0$, it is easier to aggregate higher coordinated particles as observed in (9). On the other hand, for reactivities lower than 1, lower coordination numbers are favored. For instance, samples generated with processes at a low reactivity ($w = 0.05$) the structure has above 80% of its particles as double-coordinated particles after the gelation process and above 60% after a complete aging, which means that the structure is mostly formed by long fibers. For structures generated using processes with high reactivity ($w = 1.6$) the amount of single-coordinated particles (broken ends) is about 50%, which reduces to just over 10% after complete aging. On the other hand for the range of reactivities simulated, it seems that w does not have a strong effect on the amount of triple-coordinated particles after complete aging, all the structures having between 25% and 30% of these particles.

5 Conclusions

The effect of reactivity and density on the structure of the aerogel and the link established here between these parameters, as well as the processing conditions of the *sol*, expand the possibilities for designing aerogel structures according to application requirements. The structure as gelled depends uniquely on the density and the reactivity. For instance, aerogels expected to have high thermal resistivity can be fabricated using conditions favoring high reactivity, and not allowing aging of the samples. The final structure will have a large amount of broken ends, which will create a cumbersome path for the heat to diffuse through. Another example could be the fabrication of aerogels expected to have good structural integrity, and to be able to withstand loads. For this case a structure with a small percentage of broken ends is desired; therefore a process with low

reactivity should be used. Aging and/or sintering the samples would have a positive effect on integrity, because it will increase the amount of branching points in the structure, due to an higher percentage of triple- and tetra-coordinated particles, along with a reduction of the broken ends.

References

References

Molar ratio water:alkoxide	4
Molar ratio alcohol:alkoxide	8
Completeness of reaction	ideal
Catalyst	none

Table 1: Processing conditions from **?**.

Cluster	E_c [kcal/mol]	Model 1	Model 2
q_2^1	-9.381	$2E_1$	$2(a_1 + a_2)$
$q_2^1 q_1^2$	-15.512	$2E_1 + E_2$	$2(a_1 + a_2) + (a_1 + 2a_2)$
q_3^2	4.763	$3E_2$	$3(a_1 + 2a_2)$
$q_2^2 q_2^1$	-38.146	$2E_1 + 2E_2$	$2(a_1 + a_2) + 2(a_1 + 2a_2)$
$q_3^1 q_1^3$	-30.616	$3E_1 + E_3$	$3(a_1 + a_2) + (a_1 + 3a_2)$
$q_2^2 q_1^3 q_1^1$	-4.192	$E_1 + 2E_2 + E_3$	$(a_1 + a_2) + 2(a_1 + 2a_2) + (a_1 + 3a_2)$
q_4^2	-25.715	$4E_2$	$4(a_1 + 2a_2)$
$q_3^2 q_2^1$	-43.587	$2E_1 + 3E_2$	$2(a_1 + a_2) + 3(a_1 + 2a_2)$
$q_3^1 q_1^3 q_1^2$	-40.198	$3E_1 + E_2 + E_3$	$3(a_1 + a_2) + (a_1 + 2a_2) + (a_1 + 3a_2)$
$q_4^1 q_1^4$	-31.978	$4E_1 + E_4$	$4(a_1 + a_2) + (a_1 + 4a_2)$
$q_3^2 q_1^3 q_1^1$	-20.049	$E_1 + 3E_2 + E_3$	$(a_1 + a_2) + 3(a_1 + 2a_2) + (a_1 + 3a_2)$
q_5^2	-12.582	$5E_2$	$5(a_1 + 2a_2)$

Table 2: Cluster formation energies from **?** and models.

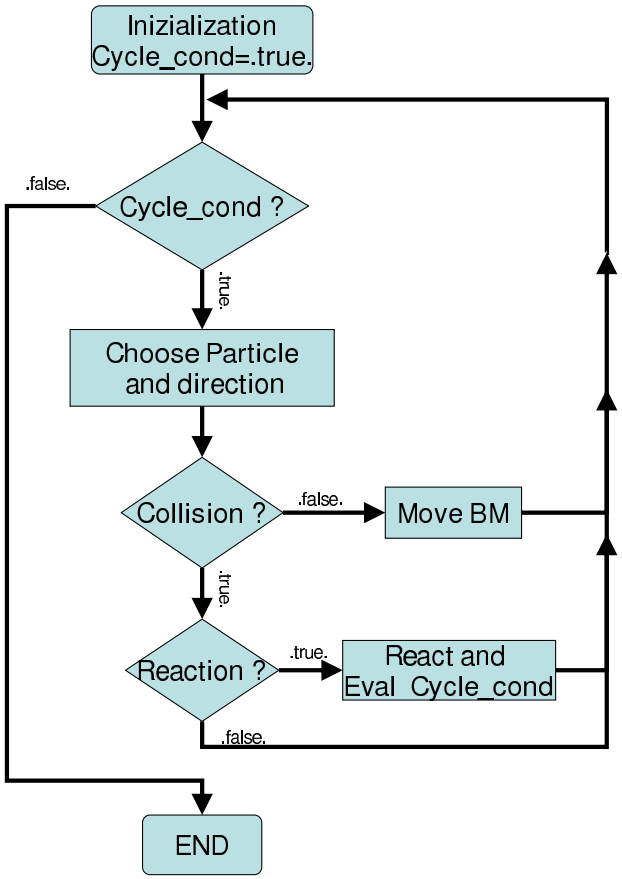

Figure 1: Flow chart of sol-gel algorithm.

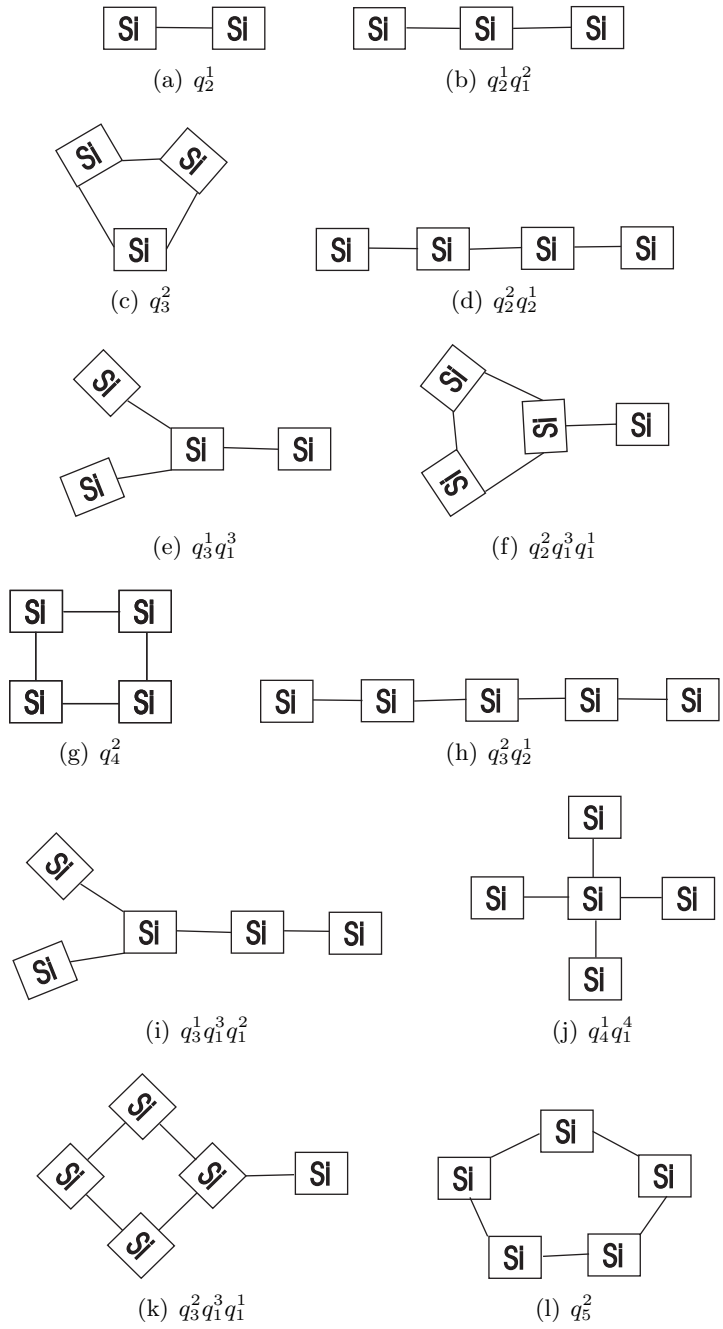

Figure 2: Geometry of the clusters modeled by **?**. Each bar represents an oxygen bond between two silicon atoms.

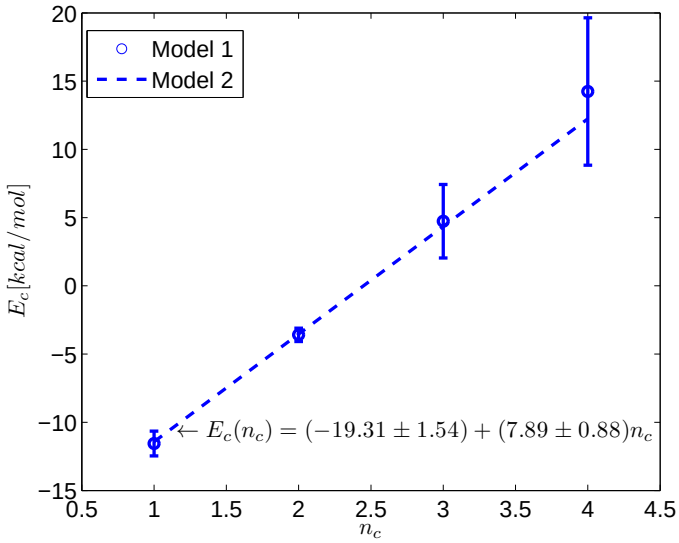

Figure 3: Energy Models

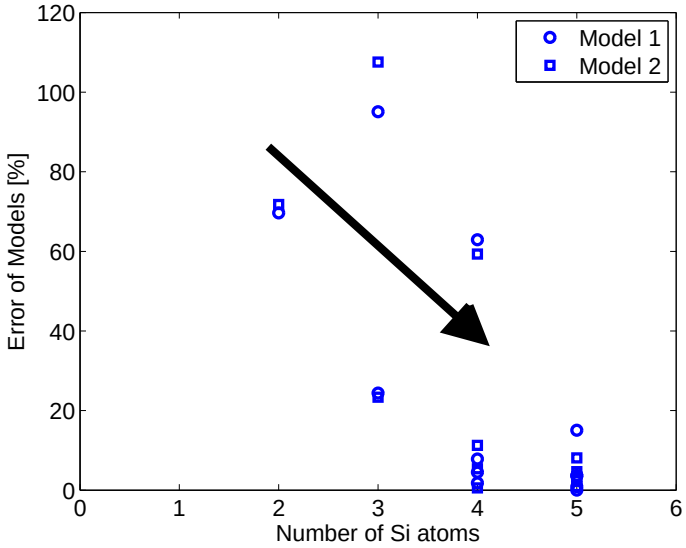

Figure 4: Error of Models compared to the values from **?**.

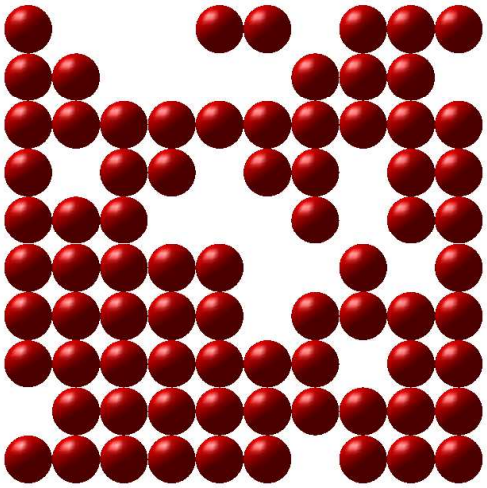

(a) $N = 251$ and $L = 10$

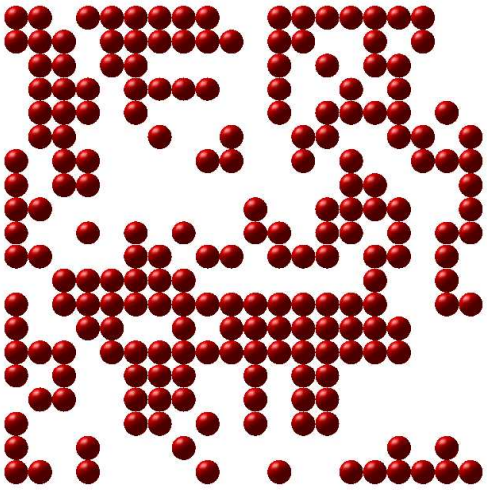

(b) $N = 1326$ and $L = 20$

Figure 5: Slice of the network for $w = 1$, and for different correlation lengths, L.

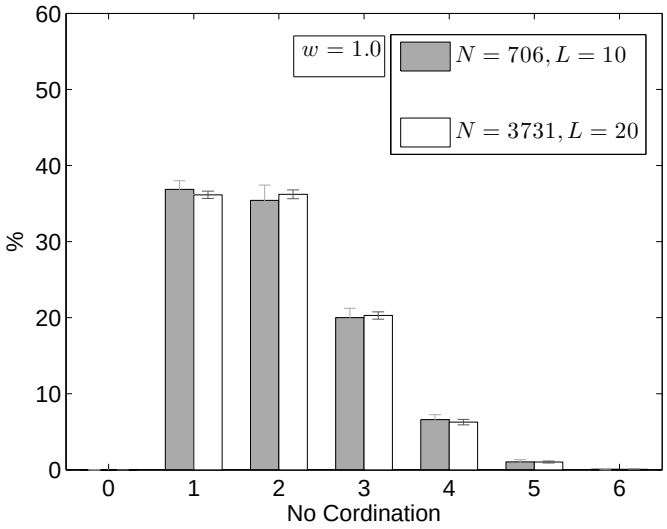

Figure 6: Coordination number distribution for $N = \{251, 1326\}$ and $L = \{10, 20\}$ with $w = 1$

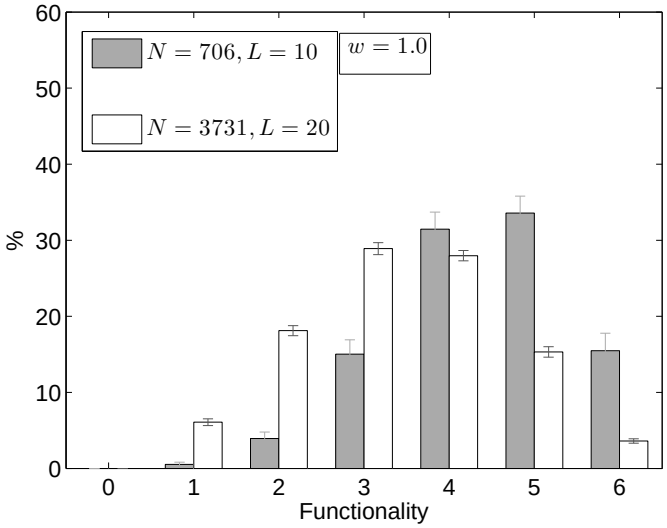

Figure 7: Functionality distribution for $N = \{251, 1326\}$ and $L = \{10, 20\}$ with $w = 1$

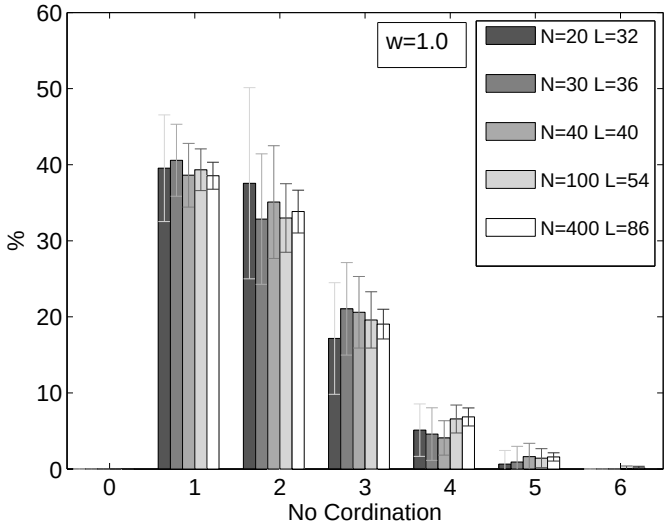

Figure 8: Coordination number distribution for different number of particles holding the same initial density.

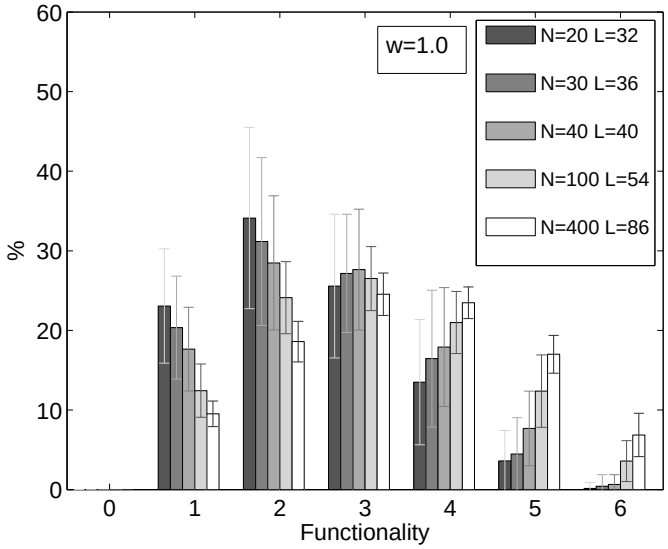

Figure 9: Functionality distribution for different number of particles holding the same initial density.

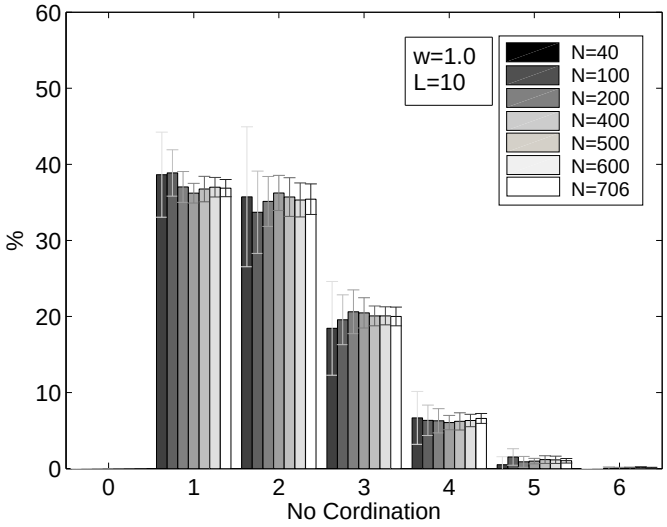

Figure 10: Coordination number distribution for several densities with $L = 10$.

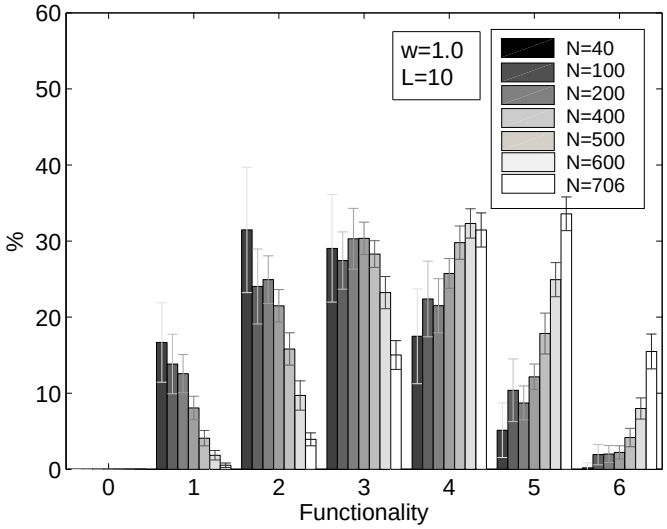

Figure 11: Functionality distribution for several densities with $L = 10$.

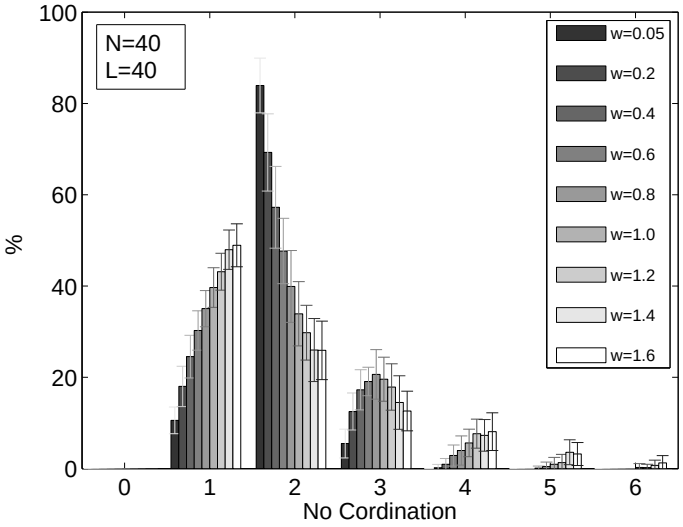

Figure 12: Coordination number distribution for several reactivities.

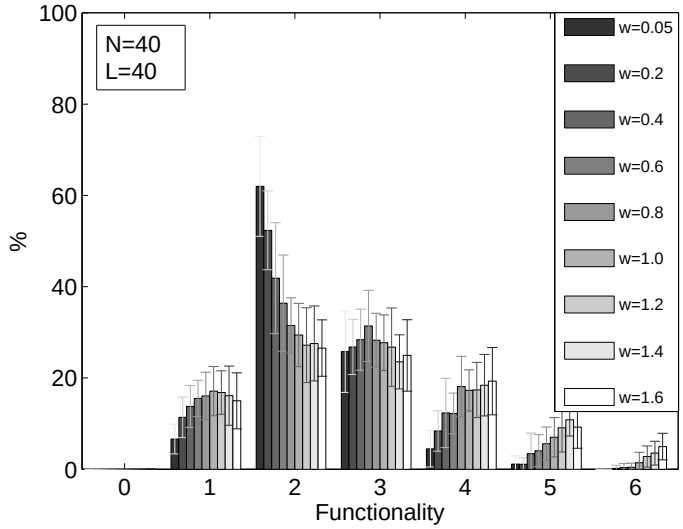

Figure 13: Functionality distribution for several reactivities.